J Paleolimnol
DOI 10.1007/s10933-009-9376-x

ORIGINAL PAPER

Records of large earthquakes in lake sediments along the North Anatolian Fault, Turkey

X. Boës · S. B. Moran · J. King · M. N. Cağatay · A. Hubert-Ferrari

Received: 13 January 2009 / Accepted: 26 August 2009

Abstract In 1999, the large surface-rupturing earthquakes of Izmit and Duzce completed a 60-year cycle that included a westward migration of nine consecutive large earthquake failures (>50 km surface rupture), which started with the 1939 Erzincan earthquake in eastern Turkey. In this study, we focused on seismic cycles and seismic risk predictability along the North Anatolian Fault (NAF). Toward the west end of the NAF (26°E–32°E, i.e. Bolu), large earthquake frequency is measured from either historic earthquake catalogs, or geologic records from isolated outcrops and marine sediment cores from the Marmara Sea. In comparison, the eastern part of the NAF zone (32°E–42°E) is less well documented by palaeo-seismologic archives. Thus, the sediment records of lake basins located on the eastern NAF zone constitute a unique opportunity for testing a new palaeo-seismologic approach. To this end, we used a diverse array of complementary methods involving: (1) a 600-km transect of fault-related lakes, (2) sedimentologic observations on cores from six lakes, and (3) a comparison between records of catastrophic sediment transfers in lakes (i.e. radionuclide chronomarkers and erosion tracers) and historic earthquake reports. Our study indicates that lakes along the NAF are sensitive geologic recorders of large surface-rupturing earthquakes (surface-wave magnitude (M_s) $\geq$ 6.9); smaller intensities are not recorded. The most responsive lake systems exhibit increases in sediment accumulation by a factor of >40 for a >3-m strike-slip displacement ($M_s \geq 7$). However, based on results from the 1939 Erzincan earthquake ($M_s = 7.8$) chronostratigraphic marker, large surface-rupturing earthquakes are detected only by certain lake records and not by others. Matching multiple lake records along the NAF provides information both on the location of a surface rupture of a paleo-earthquake as well as its magnitude. Finally, the shallow lake basins along the NAF could potentially document cycles of large seismic events for at least the late Holocene.

Keywords Europe · NAF · Tectonic · Palaeoseismology · Erzincan · Seismites · Radionuclide tracers · Geochronology

X. Boës (✉) · A. Hubert-Ferrari
Observatoire Royal de Belgique, Service de Séismologie, 1180 Uccle, Belgium
e-mail: xavierb@oma.be

S. B. Moran · J. King
Graduate School of Oceanography, University of Rhode Island, Narragansett, RI 02881, USA

M. N. Cağatay
Eastern Mediterranean Centre for Oceanography and Limnology, Department of Geological Engineering, Istanbul Technical University, 34469 Maslak, Turkey

Introduction

As a result of collision between the Arabian and Eurasian plates, the Anatolian block (Turkey) moves westward at a rate of 25 ± 5 mm/year (Westaway 1994; Reilinger et al. 1997; Armijo et al. 1999). The extrusion of Anatolia is accommodated by strike-slip faulting in the southeast and north of Anatolia (Fig. 1a; Ambraseys 1970; Barka and Kadinski-Cade 1988; Stein et al. 1997; Hubert-Ferrari et al. 2003; Sengor 2005). Due to active plate boundaries, Turkey is sensitive to surface-rupturing earthquakes. The

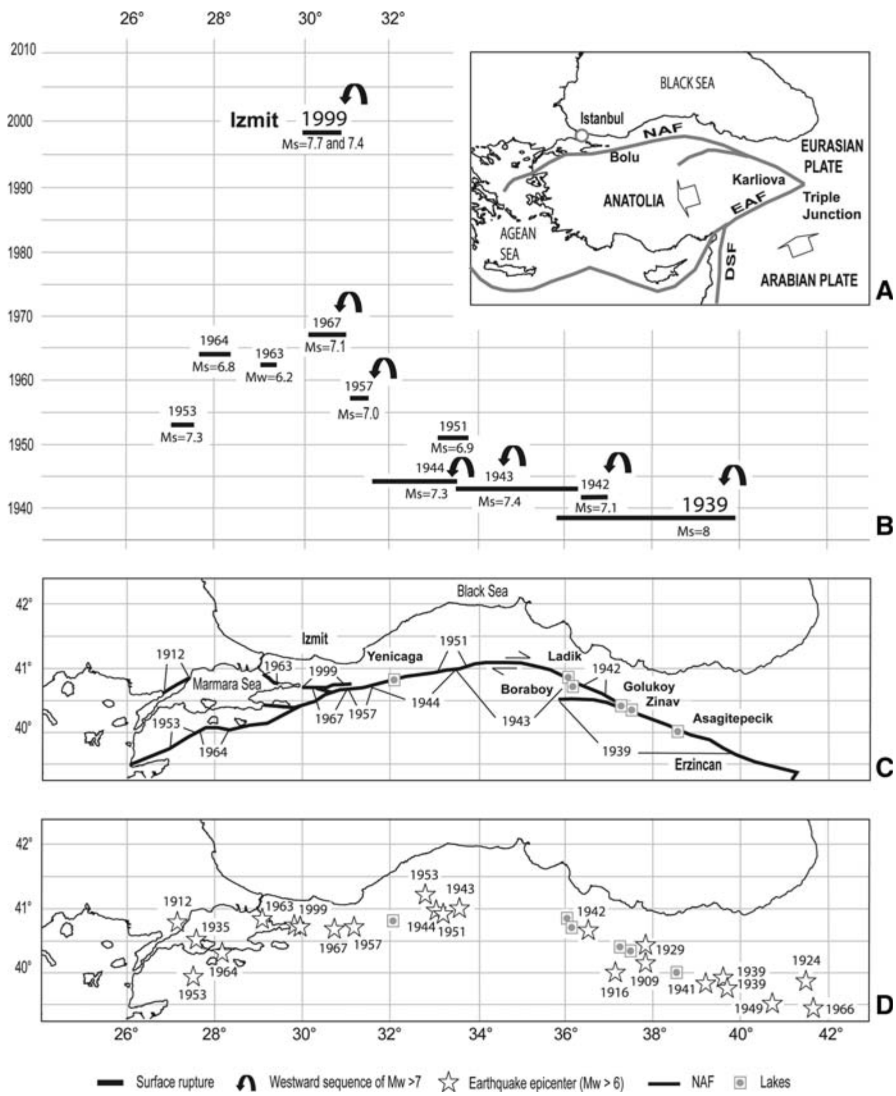

Fig. 1 **a** Study area and westward extrusion of the Anatolian block at a rate of 25 mm/year in the Sea of Marmara region (after Reilinger et al. 1997). **b** Surface rupture lengths and timing of the 1939–1999 migration sequence of large earthquakes ($M_s \geq 6.9$) along the NAF (compiled from Ambraseys 1970; Barka 1992; Ambraseys and Finkel 1995; Stein et al. 1997). **c** Ruptured fault segments ($M_s > 6$) between 1912 and 1999 (modified from Ambraseys 1970; Barka 1992, 1999; Stein et al. 1997). **d** Target lakes along the NAF and regional $M_s > 6$ epicenters for the last 150 years (compiled from Ambraseys 1970; Ambraseys and Finkel 1995; Tan et al. 2007; NOAA/NGDC data base): 1909 ($M_s = 6.4$; 40.2°N–37.8°E), 1912 ($M_s = 7.4$; 40.7°N–27.2°E, 1916 ($M_s = 7.2$; 39.8°N–37.1°E), 1924 ($M_s = 6.8$; 39.5°N–41.2°E), 1929 ($M_s = 6.5$; 40.2°N–37.9°E), 1935 ($M_s = 6.2$; 40.5°N–27.5°E), 1939 ($M_s = 8$; 39.7°N–39.7°E), 1939 ($M_s = 6$; 39.9°N–39.7°E), 1941 ($M_s = 6.0$; 39.8°N–39.3°E), 1942 ($M_s = 7.1$; 40.7°N–36.6°E), 1943 ($M_s = 7.4$; 41.0°N–34.0°E), 1944 ($M_s = 7.3$; 41.0°N–33.0°E), 1949 ($M_s = 6.9$; 39.4°N–40.8°E), 1951 ($M_s = 6.9$; 40.7°N–33.3°E), 1953 ($M_s = 7.3$; 39.9°N–27.4°E), 1953 ($M_s = 6.4$; 41.2°N–32.8°E), 1963 ($M_s = 6.2$; 40.8°N–29.1°E), 1957 ($M_s = 7.0$; 40.6°N–31.2°E), 1964 ($M_s = 6.8$; 40.3°N–28.2°E), 1966 ($M_s = 6.8$; 39.2°N–41.4°E), 1967 ($M_s = 7.1$; 40.7°N–30.7°E), and the Kocaeli-Izmit ($M_s = 7.7$; 40.7°N–29.8°E) and Düze ($M_s = 7.4$; 40.7°N–31.1°E) 1999 events (see text)

largest shocks are located along three main faults: the Dead Sea Fault (DSF—1,200 km long) in the south, the East Anatolian fault (EAF—500 km long), and the North Anatolian fault (NAF—1,300 km long; Fig. 1c). An interesting feature of the regional seismic hazard is the noticeable switching between the NAF seismic stress and the adjacent strike-slip faults (Ambraseys 1971; Hubert-Ferrari et al. 2003; Migowski et al. 2004). In the recent past, the EAF zone has shown evidence of relative inactivity, whereas the NAF zone was more active, suggesting a stress transfer along these main fault belts (Ambraseys 1971; Stein et al. 1997; Hubert-Ferrari et al. 2003). However, the long-term relationship between the transfer of seismic stress along the EAF and the propagation of large earthquakes along the NAF needs to be confirmed by construction of longer chronologies that can be obtained from earthquake-sensitive geologic archives across the NAF.

Palaeo-earthquakes are reconstructed primarily by historic sources that provide information regarding magnitude, age, location, and recurrence of past disasters back to the Roman period (Ambraseys and Jackson 1998). In northwestern Anatolia, sediment cores may provide longer palaeo-seismologic records, as demonstrated in the Marmara Sea region (Leroy et al. 2002; Polonia et al. 2004; McHugh et al. 2006; Beck et al. 2007; Armijo et al. 2005). Eastward of the Marmara Sea, paleo-seismic trenching across the NAF provides a record ~2,000 years longer than historic sources (Sugai et al. 2001; Hartleb et al. 2003, 2006; Hitchcock et al. 2003; Pantosti et al. 2008). The NAF provides a unique laboratory for palaeo-seismology because of the presence of several lakes along the 1,300-km-long fault trace that can be cored. These lakes contain useful sediment records for climate reconstructions and radiometric dating of past sedimentologic perturbations caused by earthquakes. In this context, we tested a new palaeo-seismologic reconstruction approach along the NAF segments that ruptured during the twentieth century. Although many lakes occur along the NAF and the EAF, lake sediment sensitivity to earthquakes has not yet been evaluated. This requires a comparison between historic earthquakes and their associated co-seismic features observed in lake sediments. Comparable studies of earthquake-triggered lake deposits (seismo-turbidites) have been done in some of the most active tectonic regions of the globe, including Lake Biwa in Japan (Inouchi et al. 1996; Shiki et al. 2000), the Dead Sea fault region (Marco et al. 1996; Ken-Tor et al. 2001, Migowski et al. 2004), and the Andes (Carrillo et al. 2008).

The objective of this study was to detect environmental changes in lake systems caused by earthquakes along the NAF. We briefly present an overview of the study area and tectonic setting, and then describe the target lakes and the methods, i.e. the combined sedimentologic and radiometric dating approaches, used to study environmental changes caused by historic earthquakes. Finally, we discuss how these lake records could be further utilized to reconstruct large surface-rupturing palaeo-earthquakes in Anatolia.

The North Anatolian Fault system and historic seismicity

The NAF (Fig. 1c) is a right lateral strike slip fault, which extends from the compressive triple junction (39°17′43″N, 41°07′2″E—Fig. 1a) at Karliova to the extensional Aegean Sea. The NAF is formed by a main fault trace east of 32°E, and by three sub-segments west of 32°E (Fig. 1c). A remarkable feature of the NAF is its relatively simple behavior characterized by progressive failures along the 1,300-km-long fault trend (Fig. 1b, c; Barka and Kadinski-Cade 1988; Stein et al. 1997). Due to its relatively simple faulting structure, large earthquakes along the NAF are characterized by long surface ruptures (50–350 km) associated with 1–7.5-m strike-slip displacements (Barka 1992, 1996). According to historic datasets (Fig. 1d), three cycles of surface-rupturing earthquakes have been observed back to AD 900 along the NAF zone (Ergin et al. 1967; Ambraseys 1970; Barka 1992, 1996; Ambraseys and Finkel 1995; Stein et al. 1997; Ambraseys and Jackson 1998). The last sequence of earthquakes began in 1939 (Erzincan), near the eastern termination of the NAF, and moved toward the west until 1999 (Izmit). In the eastern part of the NAF, the great 1939 Erzincan earthquake ($M_s = 7.8$; 39.7°N–39.7°E) represents the largest surface-rupturing earthquake recorded during the nineteenth and twentieth centuries in Turkey (350-km surface rupture, Fig. 1b, c). It was followed by seven large surface faulting earthquakes: in 1942 ($M_s = 7.1$; Niksar-Erbaa; 40.7°N–36.6°E), 1943 ($M_s = 7.4$; Tosya; 41.0°N–34.0°E), 1944 ($M_s = 7.3$; Bolu-Gerede; 41.0°N–33.0°E), 1951 ($M_s = 6.9$; Kursunlu; 40.7°N–33.3°E), 1957 ($M_s = 7.0$; Abant;

40.6°N–31.2°E), and 1967 ($M_s = 7.1$; Mudurnu-Adapazari; 40.7°N–30.7°E) (Fig. 1; see Ambraseys 1970; Barka and Kadinski-Cade 1988; Ambraseys and Jackson 1998; Tan et al. 2007, and NOAA-NGDC database for earthquake coordinates and magnitudes and references therein). The Kocaeli-Izmit ($M_s = 7.7$; 40.7°N–29.8°E) and Düze ($M_s = 7.4$; 40.7°N–31.1°E) 1999 events prolonged the "stress transfer cycle" along the NAF (Fig. 1b; see Barka 1999 for Izmit events description). The consecutive $M_s \geq 6.9$ shocks ruptured a total of ~1,100 km of the NAF in just 60 years. Two earlier migration sequences of large earthquakes took place in AD 967–1050 and AD 1254–1784 according to Ambraseys (1970), Ambraseys and Finkel (1987, 1995), and Stein et al. (1997).

Materials and methods

Selected lakes, coring, physical and geochemical analysis of the sediments

Natural lakes situated on the NAF, or a few km from the main fault trace, were selected as targets because they contain sediment sequences with potential records of disturbance by historic earthquakes. Between 31°40′E (Bolu) and 40°E, i.e. the less documented area, there are only six fault-related natural lakes (Fig. 2). We investigated the following lakes from east to west: Asagitepecik, Gollukoy, Zinav, Boraboy, Ladik, and Yenicaga (Table 1). At each lake, several undisturbed short cores (~80 cm long) were collected with a

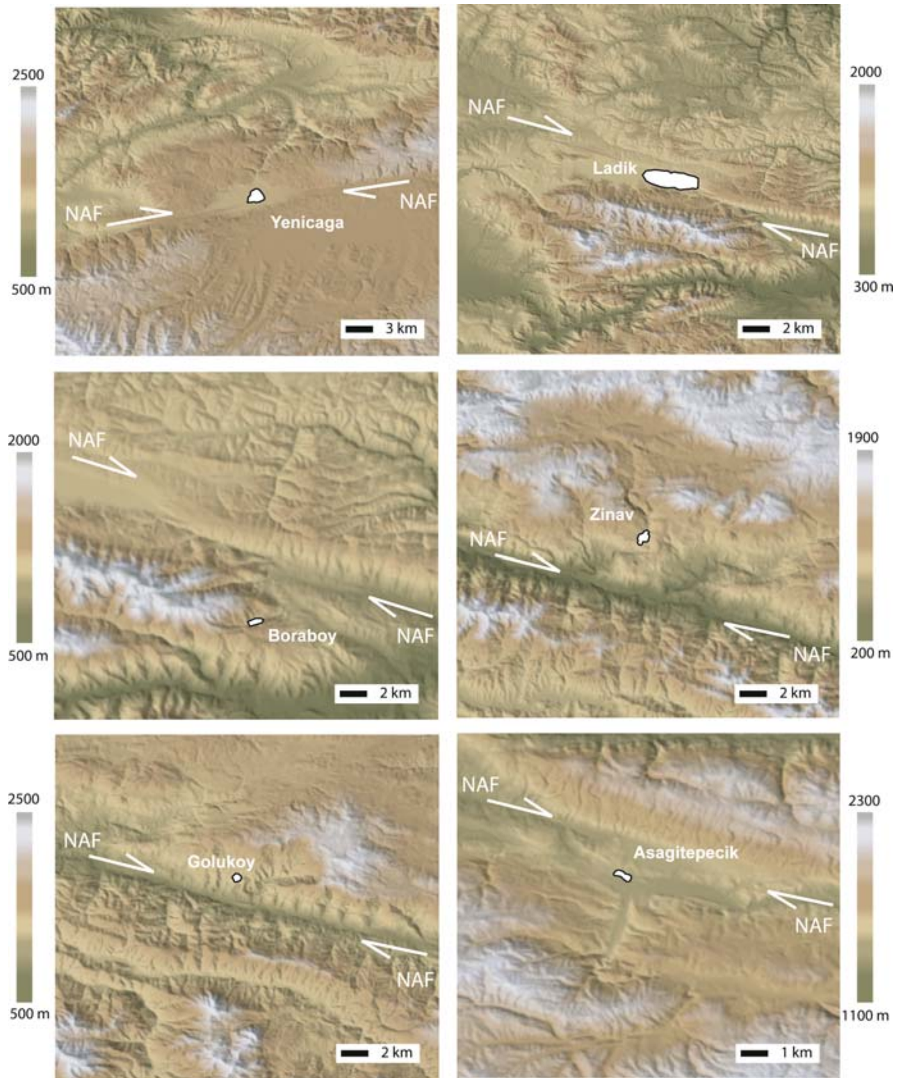

Fig. 2 Morphologic setting of lakes studied in relation to the North Anatolian Fault trace. Digital elevation models (SRTM) with data points spaced every three arc seconds (approximately 90-m resolution)

Table 1 Description of the lakes

Lakes	Coord. (degrees, minutes, seconds)	E (m)	L (m)	W (m)	A (km^2)	D (m)	Sed. rate (mm/year)	Historic earthquakes	Surface rupture (km) (Slip disp.)	Epicentre Coord. (decimal degrees)	Distance from Lake (km)	Depth in the Core (cm)	Thickness of deposit (cm)	Increase sed. Rates (by a factor of)
Asagitepecik	40°02′19 N 38°35′18E	1,266	688	189	0.10	2.3	1.5	1909 (Mw = 6.3) Zara	<50 (< 1 m)	40.20 N 37.80E	40			
								1939 (Mw = 7.8–8) Erzincan		39.70 N 39.70E	110	12–55 or 99	43 or 87	>280
								1941(Mw = 6) Erzincan	<50 (< 1 m)	39.80 N 39.30E	65	–	–	–
Gollukoy	40°22′36 N 37°28′00E	1,051	447	380	0.13	7.5	6.9	1939 (Mw = 7.8–8) Erzincan	350 (3–4 m)	39.70 N 39.70E	205	42–50	8	12
Zinav	40°26′50 N 37°16′20E	953	997	456	0.35	17	4.5	1939 (Mw = 7.8–8) Erzincan	350 (3–4 m)	39.70 N 39.70E	220	58–76	18	40
Boraboy	40°48′12 N 36°09′13E	1,082	661	160	0.08	10.5	3.6	1939 (Mw = 7.8–8) Erzincan	350 (–)	39.70 N 39.70E	330			
								1942 (Mw = 7.3) Niksar-Erbaa	50 (1.5 m)	40.70 N 36.60E	40	–	–	–
								1943 (Mw = 7.6) Tosya	265 (2.5 m)	41.ON 34.0E	190	–	–	–
Ladik	40°54′19 N 36°00′27E	868	(a) 6,869 (b) 4,900	1,925 1,020	10.38 4	2.9 <2	5.4	1939 (Mw = 7.8–8) Erzincan	350 (7.5 m)	39.70 N 39.70E	340	–	–	–
			(a) winter (b) summer					1942 (Mw = 7.3) Niksar-Erbaa	50 (1.5 m)	40.70 N 36.60E	40	–	–	–
								1943 (Mw = 7.6) Tosya	265 (2.5 m)	41.ON 34.0E	190	33–>63	>30	>55
Yenigaga	40°46′44 N 32°01′30E	989	1,723	1,590	2.15	4.4	5.7	1944 (Mw = 7.6) Bolu-Gerede	190 (3.5 m)	41.ON 33.0E	85	29–43 or 61	14 or 32	25 or 56

Regional seismicity and co-seismic structures recorded by the sediments. *E* elevation, *L* length, *W* width, *A* surface area, *D* depth. Core coordinates are listed in Table 3 modified UWITEC gravity corer. For the shallowest lake, Ladik, the corer was mounted on an extending tube. For each lake, one sediment sequence was selected based on the magnetic susceptibility, which was measured using a Bartington MS 2E system. Split sediment cores were X-rayed to study micro-lithologic variations that were not visible on the cut surface of the cores. We characterized the different lacustrine environments, i.e. geologic settings, by measuring the elemental sediment composition with an Itrax-XRF track. Finally, we measured sediment core density because palaeo-earthquakes can increase sediment transfers to lakes and thereby modify sediment density in the process. Bulk density was determined using a Geotek-GRAPE track.

Radionuclide analysis and earthquake geochronology

The chronology and mass accumulation rates in the sediment cores were established by the activity profiles of ^{210}Pb, ^{226}Ra, and ^{137}Cs. The radionuclide profiles were used to compare sediment accumulation in the different geologic settings. Radionuclide methods are commonly used to locate disturbed deposits and identify impacts of historic earthquakes in sediment cores (Arnaud et al. 2006). Samples for radiochemical analysis were collected at 1-cm intervals. Between 3 and 4 g of sediment was weighed into plastic tubes, capped with epoxy, and allowed to stand for 2–3 weeks to allow ^{226}Ra to equilibrate with ^{214}Pb. Sample heights in the tubes and counting jars were the same for all samples to ensure constant geometry for gamma spectrometry. Samples were counted using a pure Ge detector (Canberra GL20203, 150 cm^3) for ^{210}Pb, ^{226}Ra, and ^{137}Cs. The gamma energies measured were 46.5 KeV for ^{210}Pb, 352 KeV (^{214}Pb) for ^{226}Ra, and 661 KeV for ^{137}Cs. Counting efficiencies for ^{210}Pb, ^{226}Ra (^{214}Pb) and ^{137}Cs were obtained by counting sediment standards from the National Institute of Standards and Technology (NIST).

Excess ^{210}Pb activities were calculated by subtracting the average ^{226}Ra activity measured down core from the total ^{210}Pb activity, i.e. $^{210}Pb_{xs}$ = total ^{210}Pb–^{214}Pb activity. Sediment accumulation rates were estimated from the excess ^{210}Pb ($^{210}Pb_{xs}$) profiles following standard techniques used for lake sediments (Turekian and Cochran 1978; Appleby and Oldfield 1978; Appleby 1979, 2001; Carroll et al. 1995). Briefly, it was assumed that the system was at steady state and mixing by bioturbation was relatively minor. With these assumptions, there is a balance between burial and radioactive decay:

$$\omega \partial A / \partial z = -\lambda A$$

where ω is the sediment accumulation rate (cm/year), A is the excess ^{210}Pb activity (dpm/g), z is depth in the sediment column, and λ is the ^{210}Pb decay constant (0.0311/year). With the following boundary conditions: $Az = A_0$ at $z = 0$ and $Az = 0$ at $z = \infty$, the linearized solution is,

$$\ln Az = \ln Ao - (\lambda/\omega)z.$$

Thus, after subtracting the supported ^{210}Pb using the ^{226}Ra data, the linear sedimentation rate (ω) is calculated by plotting the excess ^{210}Pb against depth and estimating the slope by least squares, where $\omega = 0.0311/\text{slope}$. A logarithmic line was fit to the ln A vs. z data and the resultant slope (l/ω) used to solve for the linear sediment accumulation rate.

For each ^{210}Pb profile, the calculated ^{210}Pb ages are valid in the part of the core where sediment accumulation is relatively constant. The accumulation rate is relatively regular until the first sediment disturbance occurs. Below that level, ^{210}Pb-derived ages need to be corrected for rapidly deposited or disturbed sediments. These types of deposits are also readily detectable from the core lithology and physical property profiles, such as bulk sediment density and magnetic susceptibility. Rapid sediment transfers, or "instantaneous deposits," are well identified by sediment density increases.

Uncertainties in the radiochemically derived ages are based on counting statistics (1σ). In addition, $^{210}Pb_{xs}$-derived sediment accumulation rates were compared to the ^{137}Cs depth profiles, the latter primarily a product of atmospheric thermonuclear weapons testing since the early 1950s. By assuming that ^{137}Cs supply to the environment began in ~1954, with numerous atmospheric nuclear tests in 1963 and the Chernobyl nuclear accident in 1986 (Appleby 2008), the depths of measured ^{137}Cs peaks provide important chronostratigraphic markers. The ^{137}Cs profiles serve as an independent check on the ^{210}Pb-derived sediment accumulation rates.

Results

Lake Asagitepecik

Lake Asagitepecik (40°02′19″N–38°35′18″E, altitude 1,266 m, Fig. 2) is situated on the NAF about 230 km west of the triple junction (Fig. 1c). The lake length is 688 m and its width is about 189 m; this lake has a small surface area (0.10 km^2) and is shallow (2.3 m) (Table 1). The lake is positioned in the Pliocene zone, but its watershed encloses serpentine bedrock in the south. The lake forms a natural depression at the front of a north–south-oriented Holocene alluvial fan (Fig. 2). Lake Asagitepecik is surrounded by cultivated and irrigated lands, especially in the south. The sediment core was collected in the central basin (40°02′21″N–38°35′15″E). The core lithology is characterized by homogeneous or laminated clays. Several distinct homogeneous units are observed in the X-radiographs (Fig. 3). The main sediment components are Al_2O_3 and SiO_2 (Table 2). The sediment density varies from 1.2 to 1.5 gm/cc, with the highest values between 99 and 13 cm depth (Fig. 4). These values can be related to the banded sediment units observed in the X-radiograph (Fig. 3). The measured ^{226}Ra and total ^{210}Pb activities range from 0.7 to 1.8 dpm/g and 1.3 to 12.9 dpm/g, respectively (Table 3). $^{210}Pb_{xs}$ extends down to $\sim$13 cm (Fig. 5). For ^{137}Cs, specific activities range from 0.08 to 17.3 dpm/g (at 7.5 cm). ^{137}Cs activities below 6 cm are near the detection limit. The excess ^{210}Pb results yield a calculated sedimentation rate of 1.5 mm/year. Evidence of "sediment disturbance" is found in both the lithology and the sediment density at depths between $\sim$10 and 55 cm, or possibly down to 99 cm (Figs. 3, 4). The main deposit is characterized by a distinct, olive-brown clay unit with some lighter banded clay (Fig. 3). We also noted the presence of leaf fragments (<1 mm) in the top unit. According to the ^{210}Pb-derived age-depth scale, the date at the top

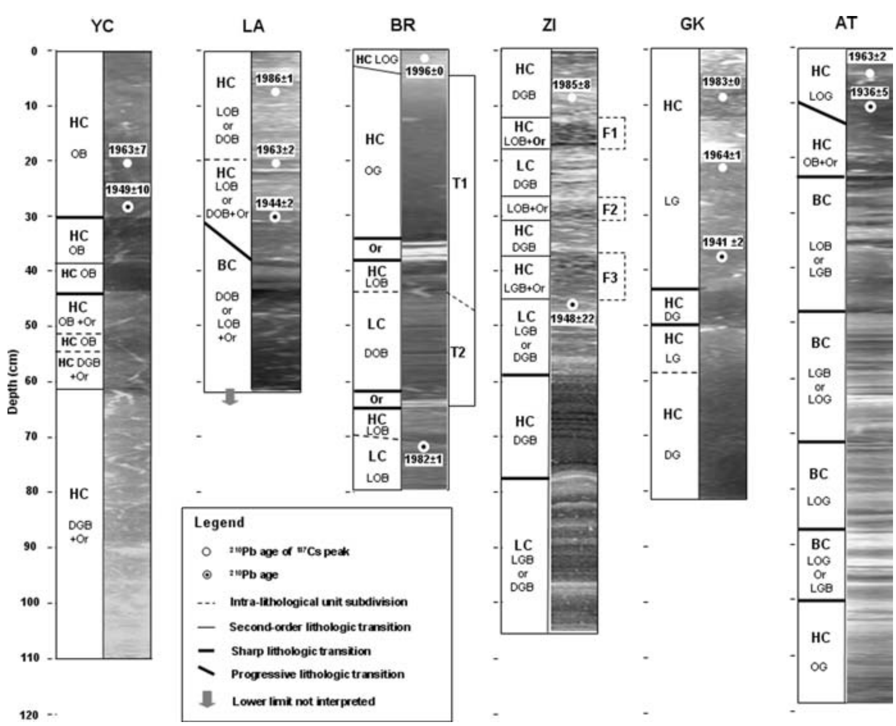

Fig. 3 Lithologic descriptions with X-radiographs of sediments collected in Lakes Yenicaga (*YC*), Ladik (*LA*), Zinav (*ZI*), Gollukoy (*GK*), and Asagitepecik (*AT*). Corrected ^{210}Pb ages reached at core base (with 1963 and 1986 ^{137}Cs geomarkers). Sedimentologic observations made by eye were validated by X-radiographs and sediment density variations in the cores (Fig. 4). F1 to F3 are interpreted as flood deposits; T1 and T2 are interpreted as modern turbidites. For Zinav, the sediment record is constructed by correlating two overlapping sediment cores. *HC* homogeneous clay, *BC* banded clays, *LC* laminated clays, *OB* olive brown, *DOB* dark olive brown, *LOB* light olive brown, *GB* grayish brown, *LG* light gray, *DG* dark gray, *DGB* dark grayish brown, *LGB* light grayish brown, *OG* olive gray, *LOG* light olive gray, *+Or* organic matter

Table 2 Elemental composition of bulk lake sediments along the NAF (by standard X-ray fluorescence track)

Lakes	Al_2O_3 (%)	SiO_2 (%)	P_2O_5 (%)	S (%)	K_2O (%)	CaO (%)	TiO_2 (%)	MnO (%)	Fe_2O_3 (%)
Asagitepecik	48.2	31	6.3	1.7	1.3	6.1	0.2	0.1	3.5
Gollukoy	29.6	35.7	4.7	1.6	3.1	19.9	0.3	0.1	3.5
Zinav	36.5	37	6	1.2	2.3	9.7	0.5	0.2	5.6
Bora boy	33.8	45.7	6.2	1.2	3.2	2.3	0.5	0.2	6
Ladik	49.6	35.4	6.2	1.3	1.3	1.5	0.3	0.1	3.6
Yenigaga	36.5	40	5.7	1.3	1.9	7.7	0.5	0.1	5

of this unit is 1936 ± 5 years (Table 4; Fig. 3). Although some uncertainty exists in the determination of the thickness of the deposit, these results suggest that sediment accumulation increased by a factor of >280 in the late 1930s (Table 1).

Lake Gollukoy

Lake Gollukoy (40°22′36″N–37°28′00″E, altitude 1,050 m, Fig. 2) lies about 100 km west of Asagitepecik (Fig. 1c). The lake has a maximum diameter of 450 m (area = 0.13 km^2) and a maximum water depth of 7.5 m (Table 1). The lake is located only 2.5 km north of the NAF (Fig. 1) and is surrounded by cultivated fields. Lake Gollukoy formed in a carbonate bedrock basin of the upper Cretaceous flysch zone and is considered a sinkhole. The core was collected in the central deep basin (40°22′39″N–37°28′10″E). The lithology is characterized by homogeneous clayey mud with one distinct homogeneous unit observed in the X-radiographs (Fig. 3). The main sediment components are SiO_2, Al_2O_3, and CaO (Table 2). In Lake Gollukoy, the bulk sediment density varies from 1.2 gm/cc to nearly 1.7 gm/cc, with the highest values between 42 and 50 cm (Fig. 4). These high values can be related to a distinct homogeneous unit observed in the X-radiographs (Fig. 3). The measured ^{226}Ra and total ^{210}Pb activities range from 1.8 to 2.4 dpm/g and 2.9 to 13.4 dpm/g, respectively (Table 3). $^{210}Pb_{xs}$ extends down to ~25 cm (Fig. 5). For ^{137}Cs, specific activities range from 0.1 to 9.2 dpm/g (at 8.5 cm). Excess ^{210}Pb results yielded a calculated sedimentation rate of 6.9 mm/year. Evidence of "sediment disturbance" is found in both the lithology and the bulk sediment density at a depth of 42 to 50 cm (Figs. 3, 4). This distinct unit is characterized by the presence of denser and darker clays (Fig. 3). The ^{210}Pb-derived date for the top of this disturbance is around the 1930s (Table 4). The calculated date at 37 cm is 1941 ± 2 years and the date at 42 cm is ~1934. Although some uncertainties exist in the determination of the thickness of the deposit, the results suggest that sediment accumulation increased by a factor of 12 in the mid 1930s (see Table 1).

Lake Zinav

Lake Zinav (40°26′50″N–37°16′20″E, altitude 953 m, Fig. 2) is situated 17 km west of Gollukoy (Fig. 1c). The lake length is 997 m, its width is about 456 m (area = 0.35 km^2) and its maximum depth is 17 m (Table 1). The lake basin is approximately 4 km north of the NAF (Fig. 2) and is surrounded by mountain rain forest. The lake formed in the upper Cretaceous flysch zone, but its watershed encloses some Eocene flysch in the north. In terms of geomorphology, Lake Zinav is interpreted as having originated by damming of a river valley. The core was collected in the northern basin of the lake (40°27′30″N–37°16′26″E). The core lithology is characterized by homogeneous to laminated clays; several distinct homogeneous units are observed in the X-radiographs (Fig. 3). The main sediment components are SiO_2, Al_2O_3, and CaO (Table 2). Bulk density varies from 1.2 to 1.6 gm/cc, with the highest values in three intervals and below 58 cm (Figs. 3, 4). These high values can be related to distinct beds observed in the X-radiographs and these correspond to lithologic changes described in detail in Fig. 3. The measured ^{226}Ra activities range from 0.5 to 2.8 dpm/g and the total ^{210}Pb activities ranges from 3.5 to 7.7 dpm/g (Table 3). $^{210}Pb_{xs}$ extends down to >50 cm (Fig. 5). For ^{137}Cs, specific activities range from 0.4 to 1.05 dpm/g (at 9.5 cm). Excess ^{210}Pb results yielded a calculated sedimentation rate of 4.5 mm/year. In Lake Zinav, several thin

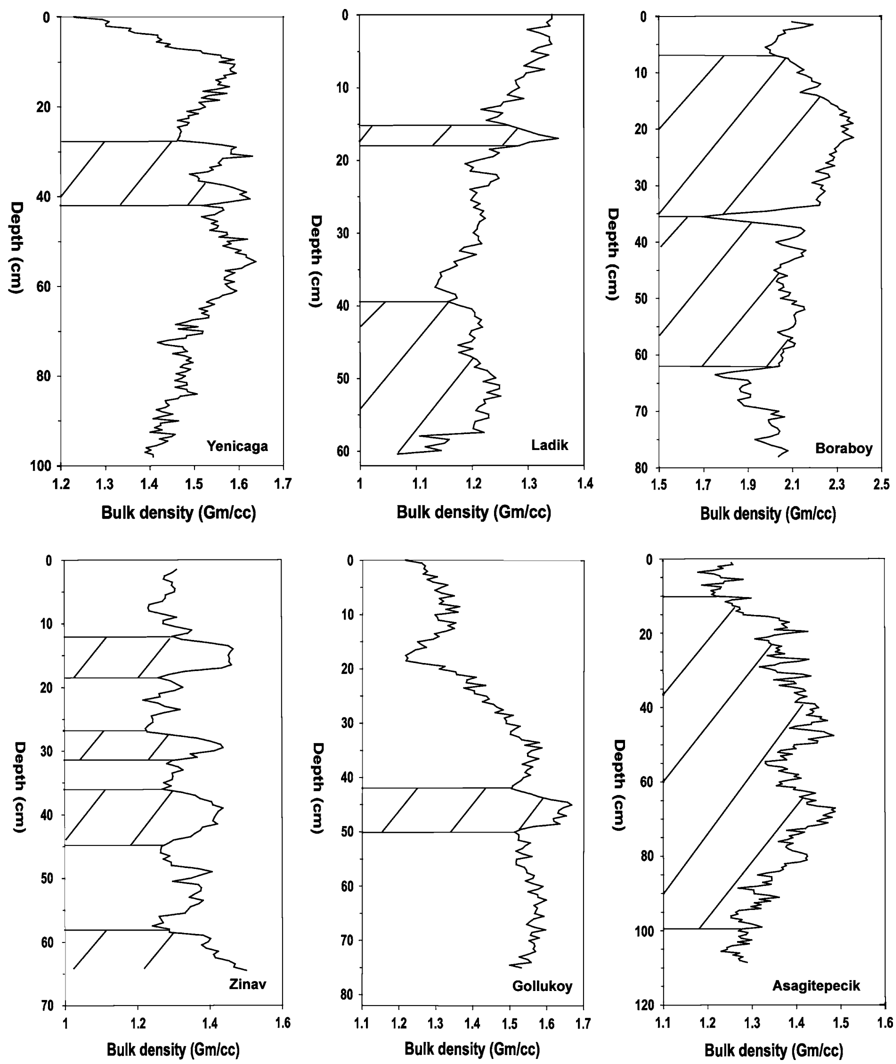

Fig. 4 Sediment bulk density profiles of the lake cores, measured using a Geotek GRAPE track. *Dashed areas* correspond to bulk density anomalies (i.e. increases in bulk density) related to disturbances observed in the lithology (Fig. 3)

beds, probably flood deposits (F1-F2-F3 in Fig. 3), are observed between the regular laminated sediments from 12 to 18 cm, 27 to 32 cm, and 36 to 45 cm. These deposits need to be subtracted prior to modeling the ^{210}Pb age (Fig. 5). Evidence of a thicker "sediment disturbance" is detected by changes in both the lithology and the bulk sediment density at a depth of 58 to 77 cm (Figs. 3, 4). This unit is characterized by very dense, dark grayish-brown clays (Fig. 3). The corrected ^{210}Pb date obtained for this abnormally thick disturbance, observed below 58 cm, is around the 1920s (see Table 4). The corrected age is 1948 $\pm$ 22 years at 46 cm and the age at 58 cm is $\sim$1922. Although some uncertainty exists in the thickness determination of the deposit, these results suggest that sediment accumulation increased by a factor of 40 in the 1920s–1930s (Table 1).

Lake Boraboy

Lake Boraboy (40°48′12″N–36°09′13″E, elevation 1,082 m, Fig. 2) is situated about 100 km west of Zinav (Fig. 1c). The lake length is 661 m, its width is 160 m (area = 0.08 km^2), and its maximum depth is $\sim$11 m (Table 1). The lake is located $\sim$5 km south of the NAF main fault trace (Fig. 2) in mountain rain forest. This lake system stands at the junction of Neogene and upper Cretaceous zones. In terms of geomorphology, Lake Boraboy is interpreted as having originated by damming of a river valley. The studied core was collected in the central basin of

Table 3 Core coordinates with sediment dry weight analyzed for total ^{210}Pb, ^{226}Ra, and ^{137}Cs determinations

Lake core	Core coordinate (D, M, S)	Sample depth (cm)	210 Pb (dpm/g)	±	226 Ra (dpm/g)	±	137 Cs (dpm/g)	±	Lake core	Core coordinate (D, M, S)	Sample depth (cm)	210 Pb (dpm/g)	±	226 Ra (dpm/g)	±	137 Cs (dpm/g)	±
AT2006 03	40°2′21.12″N	0–2	(Not measured)						BR2006 02	40°48′14.04″N	0–1	11.95	0.70	2.36	0.13	0.76	0.07
	38°35′15.00″E	4–5	12.52	0.66	1.42	0.11	14.46	0.19		36° 9′12.96″E	1–2	10.52	0.59	2.40	0.11	0.64	0.05
		5–6	9.81	0.87	1.35	0.16	11.51	0.25			3–4	5.95	0.62	2.51	0.12	0.77	0.07
		7–8	12.90	2.14	1.83	0.34	17.32	0.49			4–5	2.76	0.41	2.42	0.10	0.47	0.05
		8–9	4.66	0.64	1.27	0.12	6.99	0.17			5–6	3.48	0.26	2.57	0.07	0.55	0.03
		9–10	4.10	0.68	1.34	0.13	2.83	0.13			8–9	3.53	0.40	2.49	0.10	0.75	0.05
		11–12	3.40	0.64	1.07	0.11	0.84	0.08			14–15	3.47	0.43	2.70	0.10	0.68	0.05
		12–13	3.49	0.50	1.36	0.12	0.40	0.06			20–22	2.75	0.26	2.64	0.08	0.61	0.03
		18–19	3.31	0.49	1.05	0.08	0.19	0.05			27–28	4.73	0.42	2.57	0.10	0.78	0.05
		24–26	3.04	0.57	0.71	0.11	0.00	0.00			30–32	4.57	0.37	2.72	0.10	0.88	0.05
		34–36	1.31	0.32	1.01	0.10	0.08	0.06			43–44	8.23	0.62	3.12	0.12	1.20	0.06
											55–56	6.13	0.45	2.32	0.11	6.22	0.13
											69–70	7.88	0.55	2.29	0.11	3.77	0.09
											75–77	5.62	0.30	2.80	0.07	2.76	0.04
GK2006 03	40°22′39.36″N	0–1	13.45	0.57	1.84	0.09	6.71	0.12	LA2006 01	40°54′14.40″N	0–1	6.64	0.53	2.04	0.09	1.34	0.07
	37°28′1.20″E	3–4	12.75	0.86	2.29	0.15	8.33	0.19		36° 1′29.28″E	3–4	11.59	1.20	2.21	0.22	2.22	0.17
		8–9	8.95	0.70	2.37	0.14	9.22	0.19			5–6	7.89	0.99	2.31	0.20	2.45	0.18
		10–11	7.09	0.52	2.15	0.11	5.85	0.14			8–9	8.21	0.77	2.05	0.15	2.71	0.13
		12–13	5.46	0.47	2.44	0.11	3.24	0.08			10–11	8.31	0.97	2.42	0.21	7.35	0.37
		14–15	6.29	0.49	2.16	0.10	3.42	0.10			12–13	7.43	0.72	1.92	0.16	4.72	0.18
		20–22	5.24	0.50	2.18	0.12	4.24	0.12			14–15	9.61	1.51	2.68	0.29	3.43	0.26
		24–25	3.61	0.38	2.15	0.09	1.29	0.06			16–17	5.96	0.46	1.96	0.10	2.69	0.08
		27–28	3.88	0.37	1.93	0.09	0.35	0.04			19–20	4.38	0.53	2.03	0.13	3.21	0.12
		30–32	4.32	0.51	2.22	0.11	0.16	0.04			20–22	4.68	0.98	2.87	0.24	9.71	0.30
		36–38	2.91	0.24	2.22	0.06	0.06	0.03			25–26	8.59	1.17	1.69	0.18	2.93	0.27
											28–29	6.60	0.72	2.15	0.12	1.30	0.07
											30–32	4.31	0.67	1.46	0.14	0.50	0.07
											36–38	2.45	0.43	1.01	0.08	0.05	0.04

Table 3 continued

Lake core	Core coordinate (D, M, S)	Sample depth (cm)	210 Pb (dpm/g)	±	226 Ra (dpm/g)	±	137 Cs (dpm/g)	±	Lake core	Core coordinate (D, M, S)	Sample depth (cm)	210 Pb (dpm/g)	±	226 Ra (dpm/g)	±	137 Cs (dpm/g)	±
ZI2006 01	40°27′3.60″N	0–1	7.77	0.82	2.44	0.18	0.86	0.10	YC2006 01	40°47′3.84″N	0–1	5.61	0.59	1.67	0.12	0.61	0.06
	37°16′26.40″E	3.5–5	6.06	0.66	2.13	0.14	0.53	0.07		32° 1′35.04″E	2–3	5.94	0.47	1.74	0.10	0.67	0.06
		5–6	6.00	0.50	0.50	0.02	0.86	0.07			3–4	5.88	0.55	1.87	0.11	0.67	0.07
		9–10	5.67	0.55	1.98	0.11	1.05	0.07			4–5	5.37	0.45	1.73	0.10	1.00	0.06
		11–12	6.59	0.49	2.45	0.10	0.97	0.05			5–6	4.45	0.48	1.81	0.10	0.99	0.07
		15–16	4.61	0.42	2.79	0.11	0.39	0.05			8–9	3.48	0.44	1.91	0.11	1.21	0.07
		21–23	5.22	0.46	2.20	0.10	0.52	0.05			14–15	3.69	0.41	1.84	0.09	1.48	0.07
		28–29	4.51	0.35	1.89	0.09	0.69	0.05			18–19	3.47	0.39	1.95	0.09	1.58	0.07
		30–32	4.54	0.29	2.33	0.07	0.82	0.04			20–22	4.00	0.45	1.88	0.10	1.89	0.08
		33–34	5.27	0.26	2.28	0.05	0.86	0.03			30–32	3.25	0.26	1.87	0.06	0.78	0.04
		39–41	4.73	0.86	2.78	0.11	0.67	0.06			45–47	3.32	0.24	1.79	0.05	0.78	0.02
		45–47	3.53	0.37	1.62	0.08	0.72	0.05									

YC Lakes Yenicaga, *LA* Ladik, *ZI* Zinav, *GK* Gollukoy, *AT* Asagitepecik

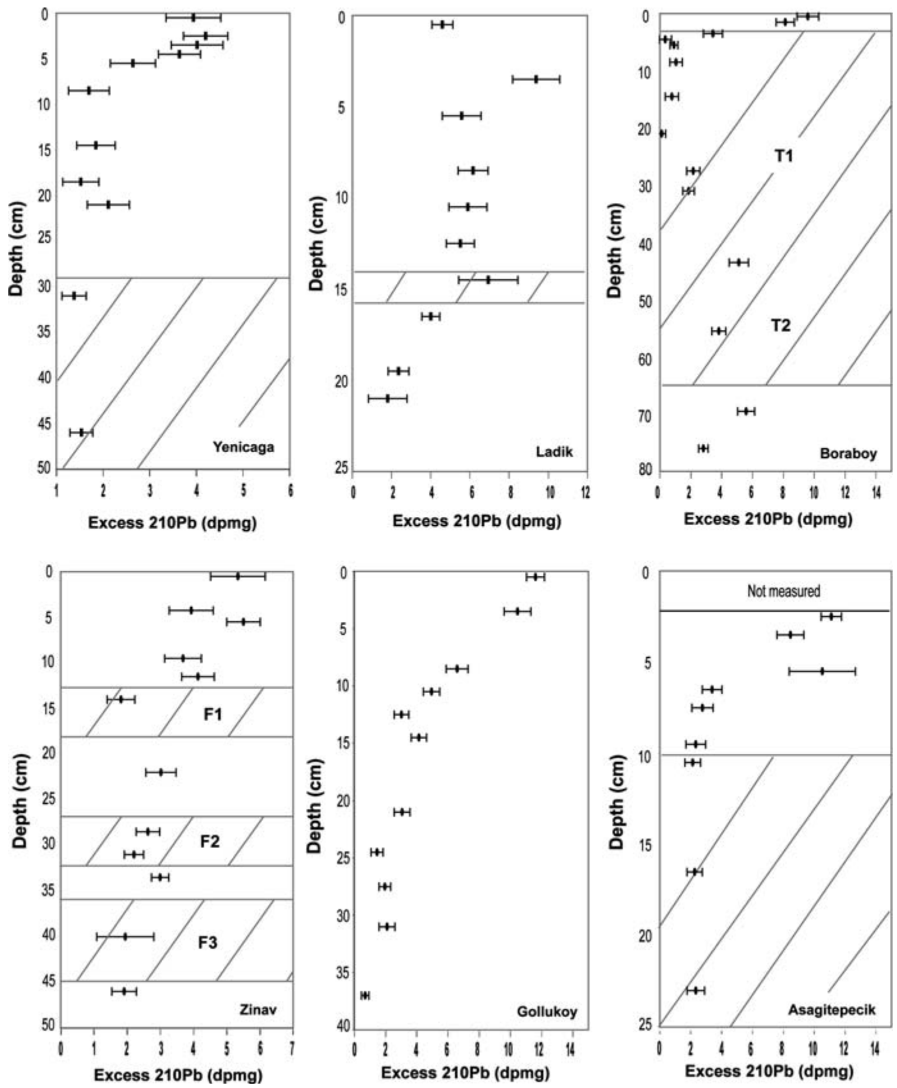

Fig. 5 Down-core profiles of ^{210}Pb activity with depth until background supported ^{210}Pb levels are reached (logarithmic fit). *Dashed areas* represent instantaneous deposits (i.e. disturbed radionuclide profiles) observed from lithologic descriptions and bulk density measurements. For Lakes Boraboy and Zinav, the age models are corrected for instantaneous deposits F1, F2, F3 and T1, T2

the lake (40°48′14″N–36°09′12″E). The lithology is characterized by homogeneous to laminated clays, with two distinct organic-rich layers associated with one laminated unit and one homogeneous thick unit, as seen in the X-radiographs (Fig. 3). The main sediment components are SiO_2 and Al_2O_3 (Table 2). Bulk sediment density varies from 1.7 gm/cc to 2.3 gm/cc, with the highest values between ~3 and 63 cm (Fig. 4). These values can be related to the two distinct units observed in the X-radiographs, which correspond to the lithologic transitions described in Fig. 3. The measured ^{226}Ra and total ^{210}Pb activities range from 2.2 to 3.1 dpm/g and 2.7 to 11.9 dpm/g, respectively (Table 3). $^{210}Pb_{xs}$ is present in two intervals, from 0 to 3.5 cm and 63 to >80 cm (Fig. 5). Specific activities of ^{137}Cs range from 0.4 to 6.2 dpm/g (at 55.5 cm). Excess ^{210}Pb results yield a calculated sedimentation rate of 3.6 mm/year. Evidence of "sediment disturbance" is detected by changes in both lithology and sediment bulk density. Sediment disturbance observed between 4 (or 8 cm) and 63 cm is characterized by denser, dark, olive-gray sediments (laminated) with two organic-rich layers and a thick homogeneous unit at the top characterized by very dense olive-gray clays (Fig. 3). The corrected ^{210}Pb age obtained for the disturbances gives an age in the 1980s and the corrected core base age is 1963 ± 2 years (Table 4).

Table 4 Sediment geochronology (^{210}Pb-derived dates with uncertainties) obtained for each study core

Lakes	Depth (cm)	Age (*AD*)	Error bar (±)	Lakes	Depth (cm)	Age (*AD*)	Error bar (±)
Asagitepecik	0–2	(Not measured)		Yenicaga	0.5	1999	0
	2.5	1983	0		2.5	1996	1
	3.5	1976	1		3.5	1994	1
	5.5	**1963**	2		4.5	1992	1
	6.5	1956	3		5.5	1990	2
	7.5	1949	4		8.5	1985	3
	9.5	1936	5		14.5	1975	5
	10.5	(1929)	6		18.5	1968	6
					21	**1963**	7
					29	1949*	10
Ladik	0.5	2001	0				
	3.5	1995	0				
	5.5	1992	0	Boraboy	0.5	1999	0
	8.5	**1986**	1		1.5	1996	0
	10.5	1982	1		3.5	1980s	–
	12.5	1979	1		4.5	1980s	–
	14.5	1975	1		5.5	1980s	–
	16.5	1971	1		8.5	1980s	–
	19.5	1966	2		14.5	1980s	–
	21	**1963**	2		21	1980s	–
	25.5	1955	2		27.5	1980s	–
	27	1952	2		31	1980s	–
	31	1944	2		43.5	1980s	–
					55.5	1980s	–
					69.5	**1981***	1
Gollukoy	0.5	1994	0		76	1963*	2
	3.5	1990	0				
	8.5	**1983**	0				
	10.5	1980	1	Zinav	0.5	2005	0
	12.5	1977	1		4.25	1997	4
	14.5	1974	1		5.5	1994	5
	21	**1964**	1		9.5	**1985**	8
	24.5	1959	1		11.5	1980	10
	27.5	1955	1		22	1970*	14
	31	1950	1		33.5	1956*	19
	37	1941	2		46	1948*	22

Bold ages are validated by independent ^{137}Cs chronomarkers (1986 and 1963 ^{137}Cs fallout events). Numbers with (*) correspond to corrected ^{210}Pb ages for instantaneous deposits

Lake Ladik

Lake Ladik (40°54′14″N–36°01′29″E, elevation 868 m, Fig. 2) is situated about 13 km northwest of Boraboy (Fig. 1c). The lake is 7 km long, 2 km wide, and <3 m deep. This lake covers an area of 10.4 km^2 and is the largest freshwater system along the study transect (Table 1). With its location on the main fault trace and elongated fault-controlled morphology (Fig. 2), the lake is interpreted as a pull-apart basin (Barka 2000). Lake Ladik is surrounded by cultivated areas and mountain rain forest, and lies at the junction of the upper Cretaceous and Eocene zones. The studied core was collected in the eastern basin of the lake (40°54′14″N, 36°01′29″E). The lithology is characterized by homogeneous to banded clays; a distinct unit is observed at the core bottom in the X-radiographs (Fig. 3). The main sediment components are Al_2O_3 and SiO_2 (Table 2). Bulk density varies from 1.1 to 1.3 gm/cc. The highest sediment density values are observed in two intervals, between 15 and 17 cm, and from ~35 cm to the base of the core (Fig. 4). These higher density values can be related to distinct sedimentary units observed in the X-radiographs and correspond to lithologic changes described in Fig. 3. The measured ^{226}Ra activities range from 1 to 2.8 dpm/g and the total ^{210}Pb activities from 2.4 to 11.6 dpm/g (Table 3). $^{210}Pb_{xs}$ extends down to ~20 cm (Fig. 5). For ^{137}Cs, specific activities range from 0.5 to 7.3 dpm/g (at 10.5 cm). Excess ^{210}Pb results yield a calculated sedimentation rate of 5.4 mm/year. Evidence of "sediment disturbance" is detected by changes in both sediment lithology and bulk density. The distinct disturbance observed below ~35 cm is characterized by denser, dark-to-light olive-brown clays enriched by organic debris (2–5 mm thick) (Fig. 3). The corrected ^{210}Pb age is ~1943 at the top of the thickest disturbed unit (Table 4). Although some uncertainty exists in the thickness determination of this deposit, these results suggest that sediment accumulation increased by a factor of >55 in the 1940s (Table 1).

Lake Yenicaga

Lake Yenicaga (40°47′30″N, 32°01′35″E, elevation 989 m, Fig. 2) is located ~340 km west of Ladik (Fig. 1c). This lake has a maximum diameter of 1.7 km (area = 2.15 km^2) and a water depth of 4.4 m (Table 1). Lake Yenicaga lies on the NAF (Fig. 2) and is interpreted to be a small pull-apart basin. The lake forms a small depression in the Cretaceous rocks, and is surrounded by irrigated, cultivated lands. The core was taken in the eastern basin of the lake (40°47′3″N, 32°01′35″E). The core lithology is characterized by homogeneous clays. Several distinct homogeneous units are observed in the X-radiographs (Fig. 3). The main sediment components are SiO_2 and Al_2O_3 (Table 2). Bulk density varies from 1.4 to 1.6 gm/cc, with the highest values between 29 and 42 cm (Fig. 4). These high values can be related to distinctly denser units observed in the X-radiographs and these correspond to lithologic transitions described in Fig. 3. The ^{226}Ra activities range from 1.7 to 1.9 dpm/g and the total ^{210}Pb activities range from 3.3 to 5.9 dpm/g (Table 3). $^{210}Pb_{xs}$ extends down to ~10 cm (Fig. 5). Specific activities of ^{137}Cs range from 0.6 to 1.8 dpm/g (at 21 cm). Excess ^{210}Pb distribution yielded a calculated sedimentation rate of 5.7 mm/year. Evidence of "sediment disturbance" is detected by changes in both core lithology and bulk density. The disturbance deposits observed between 29 and 42 cm, and possibly down to 61 cm (Fig. 4), are characterized by denser, olive-brown clays, with some organic material in the bottom unit (Fig. 3). The corrected age is 1949 ± 10 years at 29 cm and the date at the top of this thick, disturbed unit is close to 1944 (Table 4). These results suggest that sediment accumulation increased by a factor of ~50 in the 1940s (Table 1).

Discussion

Validity of the disturbed sediment geochronology

Some degree of sediment mixing is apparent in the radionuclide profiles and complicates dating and interpretation. Mixing could have been caused by wind-driven water circulation or bioturbation. Despite the evidence for sediment mixing in most of the cores, there is a near-exponential downcore decrease in the $^{210}Pb_{xs}$ data (Fig. 5). Plots of ^{137}Cs concentration against ^{210}Pb-derived ages indicate detectable ^{137}Cs in sediment extending back to the early 1950s in the lake cores (Fig. 6), except that from Boraboy, where sediments have been disturbed by "modern" turbidite deposits. Thus, the independent ^{137}Cs chronomarker in sediment since the 1950s is consistent with the ^{210}Pb-derived ages, providing further support for the calculated sediment accumulation rates in most lakes (Table 4; Fig. 6). Finally, ^{210}Pb-derived sedimentation rate estimates appear to be reasonably robust because the calculated ages of disturbances detected in the lithology agree well with the historic earthquake chronology.

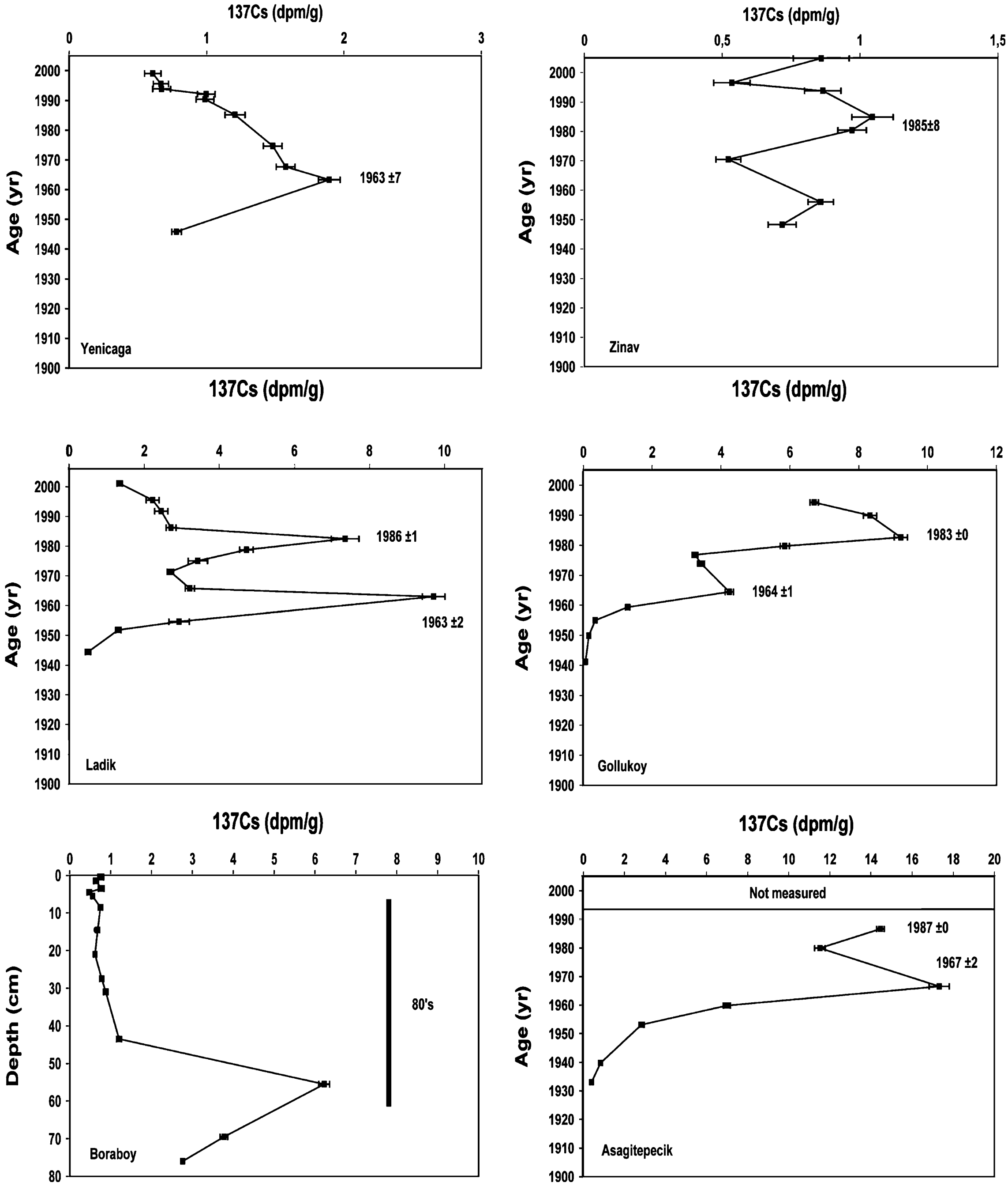

Fig. 6 Downcore ^{137}Cs profiles vs. ^{210}Pb-derived age models. ^{210}Pb dates are consistent with 1963 and 1986 maximum ^{137}Cs activities. Calculated sedimentation rates are reported for each lake (see Table 1 for details). For Lake Boraboy, due to the presence of two thick modern turbidites at the core top (i.e. reworked sediments in the 1980s), ^{137}Cs data are plotted vs. depth scale

Large-magnitude earthquake evidence in lake sediments along the NAF

Evidence of the great 1939 Erzincan ($M_s = 7.8$) in Lake Asagitepecik

The great Erzincan earthquake occurred in December 1939 and ruptured 350 km of the fault west of Erzincan. Geologic evidence of the 1939 event was expected to have been recorded in the sediments of Lake Asagitepecik since this lake is located on the 1939, ruptured-fault segment. However, three predecessors of the great 1939 earthquake are noted in historic sources (1924, 1916, and 1909; Fig. 1d), as are three earthquakes after 1939 (1941, 1949, and 1966; Fig. 1d). According to an isoseismic map (Eyidogan et al. 1991), the Asagitepecik area may have been affected by the 1909 event, but not by the other earthquakes. To summarize, throughout the twentieth century, only the large, surface-rupturing earthquakes of 1939 (and possibly 1909) were recorded in Lake Asagitepecik sediments.

Comparison of lithologic and radiochemical profiles (^{210}Pb, ^{137}Cs) suggests the presence of only one earthquake-triggered deposit that could be attributed to the 1939 event (Figs. 3, 7). Deeper in the sediments, however, the age model is not accurate because it is close to the detection limit for ^{210}Pb. Thus, despite some uncertainty, we suggest that our data indicate one event, most probably a large earthquake in the mid-twentieth century, most likely the 1939 event (Fig. 7). Historic sources report the occurrence of three large, ancient surface-rupturing earthquakes in the area: (1) AD 1254 at Susehri (40.0°N, 39.0°E; 150-km surface rupture), (2) AD 1668 at Amasya (40.5°N, 36.0°E; 400-km surface rupture), and (3) AD 1784 at Elmali (39.3°N, 40.1°E; 150-km surface rupture) (Ambraseys and Jackson 1998). These earthquakes occurred too long ago to be recorded in the short cores from this study.

Evidence of the great 1939 Erzincan ($M_s = 7.8$) earthquakes in Lakes Gollukoy and Zinav

For Lakes Gollukoy and Zinav, only the great 1939 Erzincan earthquake was expected to be identifiable based on known regional seismic activity and the isoseismic map (Table 1). These two lakes stand on the western side of the 1939 rupture. According to the lithology, radionuclide profiles, and ^{210}Pb-derived

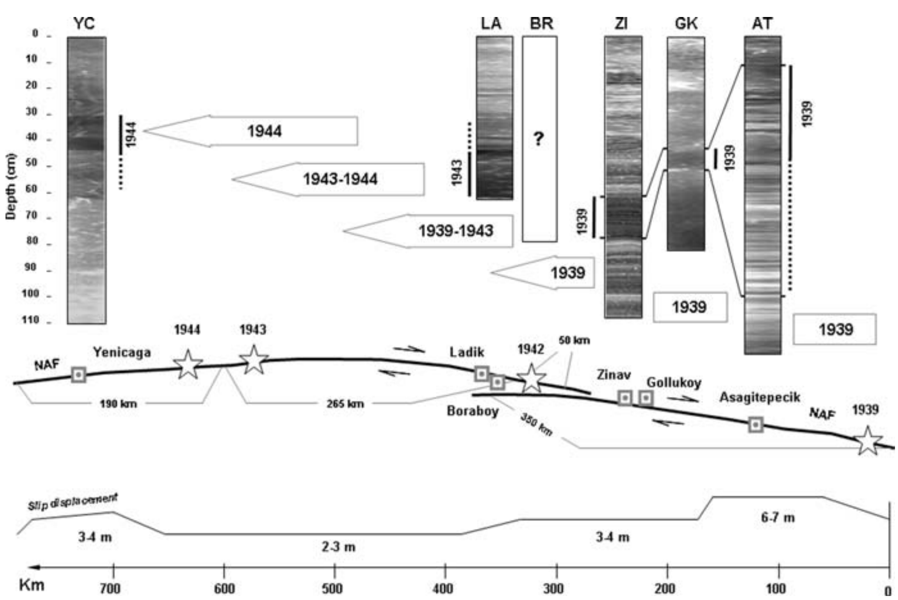

Fig. 7 Spatial-temporal distribution of chronostratigraphic marker layers attributed to 1944, 1943, and 1939 large earthquakes ($M_s > 6.9$). The spatial–temporal distributions of the 1939 deposit in Lakes Asagitepecik, Gollukoy and Zinav suggest a minimum surface rupture of 110 km (equivalent to $M_s > 7$). The cumulative surface rupture between 1939 and 1944 is 620 km. Slip displacements are reported after Barka (1996). Therefore, the spatial–temporal distribution of equivalent chronostratigraphic markers along the NAF could potentially document large surface-rupturing earthquake cycles

age models, the 1939 event can be clearly identified in both cores (Fig. 3). In these lakes, there is some uncertainty regarding the thickness of the 1939 chronostratigraphic marker (Fig. 3). This event can be identified with confidence at Lake Gollukoy, where an 8-cm-thick unit with a ^{210}Pb date of about 1934 occurs at a depth of 42 cm (Fig. 3). In Lake Zinav, an 18-cm-thick "instantaneous" deposit is observed at a depth of 58 cm (Fig. 3) and can be interpreted as a consequence of the 1939 earthquake, according to the ^{210}Pb age model (i.e. the ^{210}Pb-derived age, corrected for episodic flood deposits; Table 4; Fig. 7). These two lake systems reveal different accumulation rates for the 1939 event, though both lakes are located at nearly the same distance from the ruptured fault segment.

Evidence of the 1939, 1942 and 1943 earthquakes ($M_s > 7$) in Lakes Boraboy and Ladik

Lake Boraboy is close to several ruptured fault segments: (1) the 1939 segment (Kelkit-Ezinepazar), which is located 30 km south (Amasya; Fig. 7); but the rupture near Boraboy was less important than further east (1 m vs. 5–7 m; Barka 1992), (2) the western extremity of the 1942 segment (Niksar to near Erbaa), which is located just 30 km east of Boraboy (Fig. 7); however, the 1942 earthquake had a smaller magnitude than the one in 1943 (Barka and Kadinski-Cade 1988), and (3) the 1943 segment is 5 km north (Destek) (Fig. 7; Table 1). Based on our sediment core data, there is no evidence of these historic earthquakes. Two "turbidites" (T1 and T2; Fig. 3) are observed in the core, however these occur in the 1980s based on ^{210}Pb and ^{137}Cs measurements (Table 3; Figs. 5, 6). According to our data, the two turbidites are only 20–25 years old and coincide with the construction of a dam. The deposits appear to be unrelated to the 1943, 1942 or 1939 earthquakes. Since the two observed deposits do not match historic earthquakes, they must have originated from processes other than seismo-tectonic activity. These lakes contain evidence of older earthquakes, but deeper in the sediment (Avsar et al. 2009).

Lake Ladik stands on the 1943, ruptured segment and close to the 1939 and 1942 ruptured fault segments (Fig. 1). Lithologic descriptions and sediment density (Figs. 3, 4) identify a distinct sedimentary structure below 33 cm. The ^{210}Pb-derived date at the top of the unit, 1944 ± 2 years at 31 cm, suggests a good correlation with the historic earthquake chronology. The deposit could be related to the 1943 Tosya earthquake ($M_s = 7.4$). The thick deposit could be explained by the fact that Lake Ladik is a pull-apart basin situated on the 1943 ruptured segment, whereas the 1939 and 1942 ruptured segments are more than 30 km from the lake.

Evidence of the 1944 earthquake ($M_s = 7.3$) in Lake Yenicaga

The Yenicaga area was shocked in 1944, 1951, 1957, and 1967 (Fig. 1d). However, Lake Yenicaga is located too far from these earthquake centers, except the 1944 earthquake of Bolu-Gerede ($M_s = 7.3$), which could potentially be represented in the lacustrine sequence. Lake Yenicaga lies on the 1944 segment. Additionally, the Kocaeli and Düze earthquakes could not have disturbed Lake Yenicaga sediments because the lake is >50 km east of the westernmost 1999 surface ruptures (Fig. 1c). Based on the lithology and ^{210}Pb-derived ages (Fig. 3), the 1944 event can be clearly associated with the main disturbance observed in the core. Our data also show a period of inactivity in this portion of the NAF, from before the mid-nineteenth century to 1944. This conclusion is supported by historic reports that indicate that the area was relatively inactive for ~270 years, with the only major event in the region prior to the 1944 earthquake occurring in AD 1668 (Ambraseys and Jackson 1998).

Implications for palaeo-seismology: the spatial–temporal distribution of earthquake deposits in lake sediments along the NAF

According to the detailed lithologies, physical sediment properties, and sediment accumulation studies, it is not possible to reconstruct past earthquake magnitudes from a single, isolated geologic archive. There is not a linear relation between the thickness of earthquake deposits and earthquake magnitude in a lacustrine sediment sequence. This is due to the fact that surface ruptures are not recorded in one lake sequence and lakes lie at different distances from earthquakes. Our data from the great 1939 Erzincan earthquake, however, suggest that surface rupture length can be estimated from the spatial–temporal distribution of earthquake marker layers in multiple lake records. In terms of palaeo-seismology, these results suggest that multiple lake sediment records across the NAF could potentially document past surface-rupturing events and their cycles.

To reconstruct cycles of large surface-rupturing earthquakes, we need to construct an earthquake database from transects of lakes and other geologic records. As large earthquakes produce large surface ruptures, it will be necessary to study earthquake chronostratigraphic markers along the NAF (Fig. 7). Only a spatial–temporal study of multiple geologic archives will be relevant in terms of palaeo-seismology. In the case of the great 1939 Erzincan earthquake, only Lakes Asagitepecik, Gollukoy and Zinav recorded the event (Figs. 3, 7). Based on our compiled observations, we can reconstruct a minimum surface rupture of 110 km in 1939 (Fig. 7), and this reconstructed rupture surface is equivalent to $M_s \geq 7$. By comparison with historic reports, we know that the great Erzincan earthquake of 26 December 1939 had a surface wave magnitude of 7.8. Based on this approach, large events (i.e. $M_s > 7$ with >100 km surface rupture) could be reconstructed only by matching multiple geologic records. In addition, the spatial–temporal distribution of other chronostratigraphic markers along the NAF in 1943 (Lake Ladik) and in 1944 (Lake Yenicaga) indicates a cumulative surface rupture of 620 km in just 5 years (Fig. 7). The best palaeo-seismological reconstructions would be obtained with 50–100 km, equidistant geologic records along the 1,300 km NAF. Finally, a single study site provides limited information in terms of earthquake recurrence time.

Conclusions

Over the last decade, following the 1999 Izmit disaster (>17,000 causalities), a number of geologic and palaeo-seismologic studies have been conducted in Turkey, primarily near the west end of the NAF region and in the vicinity of Istanbul where the population is dense (>10 million people in 2009). By comparison, the eastern segment of the NAF has been less studied in terms of palaeo-seismologic reconstructions. To better understand the mechanisms behind the seismic cycles along the 1,300-km-long NAF, analyses of past seismic activity are required from geologic archives and in different regions of Anatolia. In this context, lakes constitute a new palaeo-seismological approach in this tectonically active region of the globe.

To contribute to the palaeo-seismological studies along the NAF, we studied the spatial–temporal distribution of sedimentary structures in cores recovered from six lakes along the NAF zone, from east of Bolu to Erzincan. This part of the NAF is characterized by large surface ruptures, such as the great 1939 Erzincan earthquake (350-km surface rupture). To constrain palaeo-seismologic interpretations, sediment accumulation rates were determined using ^{210}Pb-derived age models, to identify historic earthquake deposits. While there has been a small amount of mixing and diffusion in all cores, ^{210}Pb-derived accumulation rates are generally consistent with the independent ^{137}Cs chronomarker. Based on sedimentologic descriptions, sediment density, and radiochemical profiles, all lakes appear to have been significantly influenced by palaeo-earthquakes. Deposits of the twentieth century, linked to $M_s > 6.9$ shocks, displayed more than tenfold increases in sediment accumulation. However, a single lake record provides no linear relation between the thickness of the earthquake deposit and earthquake magnitude. Finally, based on the occurrence of the 1939 Erzincan earthquake ($M_s = 7.8$) chronostratigraphic marker in different lakes, this study demonstrates the utility of a spatial–temporal approach in palaeo-seismology. Future studies are required to obtain long-term earthquake records, and to match the well-dated events from different types of archives along the NAF (e.g. lake cores, outcrops, trenches, drill holes). These multiple records could be used to reconstruct the surface rupture of paleo-earthquakes and provide insights into the associated seismic cycle/risk assessment in Turkey.

Acknowledgments This study was carried out within the framework of the EC FP6 Marie Curie Excellence Grant project titled *Understanding the irregularity of seismic cycles: A case study in Turkey*. We are grateful to the European Commission, *Human Resources and Mobility* for funding. The Fulbright commission is acknowledged for providing a grant to XB for studies at the University of Rhode Island. We thank the Eastern Mediterranean Centre for Oceanography and Limnology (EMCOL) at the Technical University of Istanbul for providing laboratory facilities, for assisting in summer field campaigns, and for XRF elemental analysis. Special thanks are due to the EMCOL personnel and students:

Celal Somuncuoğlu, Emre Damci, Dursun Acar, and Sena Akcer. We acknowledge the contribution of Ulas Avsar (University of Gent), David Garcia (ROB), and Sevgi Altinok (University of Eskisehir). We also thank Roger Kelly, Scott Stachelhaus, Danielle Cares and Chip Heil of the Graduate School of Oceanography, University of Rhode Island, for assistance in radionuclide analysis and analysis of physical sediment properties. Finally, thanks are due to Chantal Tribolo for consultation.

References

Ambraseys NN (1970) Some characteristic features of the Anatolian fault zone. Tectonophysics 9:143–165

Ambraseys NN (1971) Value of historical records of earthquakes. Nature 232:375–379

Ambraseys NN, Finkel CF (1987) Seismicity of Turkey and neighbouring regions, 1899–1915. Annales geophysicae. Series B. 5:701–725

Ambraseys NN, Finkel C (1995) The Seismicity of Turkey and adjacent areas. A historical review, 1500–1800. Eren, Istanbul, Turkey, p 240

Ambraseys NN, Jackson JA (1998) Faulting associated with historical and recent earthquakes in the eastern Mediterranean region. Geophys J Int 132:390–406

Appleby PG (1979) ^{210}Pb dating of annually laminated lake sediments from Finland. Nature 280:53–55

Appleby PG (2001) Chronostratigraphic techniques in recent sediments. In: Last WM, Smol JP (eds) Tracking environmental change using lake sediments. Basin analysis, coring and chronological techniques, vol 1. Kluwer Academic, Dordrecht, pp 171–203

Appleby PG (2008) Three decades of dating recent sediments by fallout radionuclides: a review. Holocene 18:83–93

Appleby PG, Oldfield F (1978) The calculation of lead-210 dates assuming a constant rate of supply of unsupported ^{210}Pb to the sediment. Catena 5:1–8

Armijo R, Meyer B, Hubert A, Barka A (1999) Westward propagation of the North Anatolian Fault into the northern Aegean; timing and kinematics. Geology 27:267–270

Armijo R, Pondard N, Meyer B, Uçarkus G, Mercier De Lépinay B, Malavieille J, Dominguez S, Gutscher MA, Schmidt S, Beck C, Cagatay N, Cakir Z, Imren C, Eris K, Natalin B, Özalaybey S, Tolun L, Lefèvre I, Seeber L, Gasperini L, Rangin C, Emre O, Sarikavak K (2005) Submarine fault scarps in the sea of Marmara pull-apart (North Anatolian Fault): implications for seismic hazard in Istanbul. Geochem Geophy Geosy Q06009:6–29

Arnaud F, Magand O, Chapron E, Bertrand S, Boës X, Mélières MA (2006) Radionuclide profiles (^{210}Pb, ^{137}Cs, ^{241}Am) as a help for dating recent sediments in highly active geodynamic settings (Lakes Puyehue and Icalma, Chilean Lake District). Sci Total Environ 366:837–850

Avsar U, Hubert-Ferrari A, Fagel N, Boës X, and Schmidt S (2009) Paleolimnological and sedimentological traces of the 1943 (Ms = 7.3) Earthquake in the sediments of Ladik Lake, Samsun/Turkey EGU, European Geosciences Union General Assembly 2009. Vienna, Austria, April 2009

Barka AA (1992) The North Anatolian fault zone. Annales Tectonicae 6:164–195

Barka AA (1996) Slip distribution along the North Anatolian fault associated with the large earthquakes of the period 1939 to 1967. B Seismol Soc Am 86:1238–1254

Barka AA (1999) The 17 August 1999 Izmit Earthquake. Science 285:1858–1859

Barka AA (2000) Tectonic evolution of the Niksar and Tasova-Erbaa pull-apart basins, North Anatolian Fault Zone: their significance for the motion of the Anatolian block. Tectonophysics 322:243–264

Barka AA, Kadinski-Cade K (1988) Strike-slip fault geometry in Turkey and its influence on earthquake activity. Tectonics 7:663–684

Beck C, Mercier de Lépinay B, Schneider JL, Cremer M, Çağatay N, Wendenbaum E, Boutareaud S, Ménot G, Schmidt S, Weber O, Eris K, Armijo R, Meyer B, Pondard N, Gutscher MA, Turon JL, Labeyrie L, Cortijo E, Gallet Y, Bouquerel H, Gorur N, Gervais A, Castera MH, Londeix L, de Rességuier A, Jaouen A (2007) Late Quaternary co-seismic sedimentation in the sea of Marmara's deep basins. Sediment Geol 199:65–89

Carrillo E, Beck C, Audemard MF, Moreno E, Ollarves R (2008) Disentangling Late Quaternary climatic and seismo-tectonic controls on Lake Mucubaji sedimentation (Mérida Andes, Venezuela). Paleogeogr Paleoclim Paleoecol 259:284–300

Carroll JL, Lerche I, Abraham JD, Cisar DJ (1995) Model-determined sediment ages from ^{210}Pb profiles in un-mixed sediments. Nucl Geophys 9:553–565

Ergin K, Guclu U, Uz Z (1967) A catalogue of earthquakes for Turkey and surrounding area. Publ. Techn. Univ. Istanbul, Turkey, p 169

Eyidogan H, Güçlü U, Utku Z, Degirmenci E (1991). Türkiye Büyük Depremleri Makro-Sismik Rehberi (1900–1988), ITÜ MF Jeofizik Mühendisligi Bölümü Yayınları s 200

Hartleb RD, Dolan JF, Akyüz HS, Yerli B (2003) A 2000-year-long paleoseismologic record of earthquakes along the central North Anatolian Fault, from trenches at Alayurt, Turkey. B Seismol Soc Am 93:1935–1954

Hartleb RD, Dolan JF, Kozaci O, Akyüz HS, Seitz GG (2006) A 2500-year-long paleoseismologic record of large, infrequent earthquakes on the North Anatolian fault at Çukurçimen, Turkey. GSA Bulletin 118:823–840

Hitchcock C, Altunel E, Barka A, Bachhuber J, Lettis W, Helms J, Lindvall S (2003) Timing of late holocene earthquakes on the Eastern Düzce Fault and implications for slip transfer between the southern and northern strands of the North Anatolian Fault System, Bolu, Turkey. Turk J. Earth Sci 12:119–136

Hubert-Ferrari A, King G, Manighetti I, Armijo R, Meyer B, Tapponnier P (2003) Long-term elasticity in the continental lithosphere; modelling the Aden Ridge propagation and the Anatolian extrusion process. Geophys J Int 153:111–132

Inouchi Y, Kinugasa Y, Kumon F, Nakano S, Yasumatsu S, Shiki T (1996) Turbidites as records of intense palaeoearthquakes in Lake Biwa, Japan. Sediment Geol 104:117–125

Ken-Tor R, Agnon A, Enzel Y, Stein M, Marco S, Negendank JFW (2001) High-resolution geological record of historic earthquakes in the Dead Sea basin. J Geophys Res 106:2221–2234

Leroy S, Kazancı N, Ileri O, Kibar M, Emre O, McGee E, Griffiths HI (2002) Abrupt environmental changes within a late Holocene lacustrine sequence south of the Marmara Sea (Lake Manyas, N-W Turkey): possible links with seismic events. Mar Geol 190:531–552

Marco S, Stein M, Agnon A, Ron H (1996) Long-term earthquake clustering: a 50,000-year paleoseismic record in the Dead Sea Graben. J Geophys Res 101:6179–6191

McHugh CMG, Seeber L, Cormier MH, Dutton J, Cagatay N, Polonia A, Ryan WBF, Gorur N (2006) Submarine earthquake geology along the North Anatolia Fault in the Marmara Sea, Turkey: a model for transform basin sedimentation. Earth Planet Sc Lett 248:661–684

Migowski C, Agnon A, Bookman R, Negendank JFW, Stein M (2004) Recurrence pattern of Holocene earthquakes along the Dead Sea transform revealed by varve-counting and radiocarbon dating of lacustrine sediments. Earth Planet Sc Lett 222:301–314

Pantosti D, Pucci S, Palyvos N, De Martini PM, D'Addezio G, Collins PEF, Zabci C (2008) Paleoearthquakes of the Düzce fault (North Anatolian Fault Zone): insights for large surface faulting earthquake recurrence. J Geophys Res 113:1–20

Polonia A, Gasperini L, Amorosi A, Bonatti E, Bortoluzzi G, Çagatay N, Capotondi L, Cormier MH, Gorur N, McHugh C, Seeber L (2004) Holocene slip rate of the North Anatolian Fault beneath the Sea of Marmara. Earth Planet Sc Lett 227:411–426

Reilinger RE, McClusky SC, Oral MB, King W, Toksöz MN (1997) Global positioning, system measurements of present-day crustal movements in the Arabian-Africa-Eurasia plate collision zone. J Geophys Res 102:9983–9999

Sengor AMC (2005) The North Anatolian Fault: a new look. Annu Rev Earth Pl Sc 33:37–112

Shiki T, Kumon F, Inouchi Y, Kontani Y, Sakamoto T, Tateishi M, Matsubara H, Fukuyama K (2000) Sedimentary features of the seismo-turbidites, Lake Biwa, Japan. Sediment geol 135:37–50

Stein RS, Barka AA, Dieterich JH (1997) Progressive failure on the North Anatolian fault since 1939 by earthquake stress triggering. Geophys J Int 128:594–604

Sugai T, Awata Y, Toda S, Emre Ö, Dogan A, Ozalp S, Haraguchi T, Kinoshita H, Takada K, Yamaguchi M (2001) Paleoseismic investigation of the 1999 Düzce earthquake fault at Lake Efteni, North Anatolian fault system, Turkey. Annual Report on Active Fault and Paleoearthquake Researches No. 1. Active Fault Research Center, Japan, pp 339–351

Tan O, Tapirdamaz MC, Yoruk A (2007) The earthquake catalogues for Turkey. Turk J of Earth Sci 17:405–418

Turekian KK, Cochran JK (1978) Determination of marine chronologies using natural radionuclides. In: Riley JP, Chester R (eds) Chemical oceanography, vol 7. Academic Press, New York, pp 313–360

Westaway R (1994) Present-day kinematics of the Middle-East and Eastern Mediterranean. J Geophys Res 99:12071–12090